

## ON THE RADIAL DISTRIBUTION OF HORIZONTAL BRANCH STARS IN NGC 2808<sup>1</sup>

G. IANNICOLA<sup>2</sup>, M. MONELLI<sup>3</sup>, G. BONO<sup>2,4</sup>, P.B. STETSON<sup>5</sup>, R. BUONANNO<sup>4</sup>, A. CALAMIDA<sup>6</sup>, M. ZOCCALI<sup>7</sup>, F. CAPUTO<sup>2</sup>,  
M. CASTELLANI<sup>2</sup>, C.E. CORSI<sup>2</sup>, M. DALL'ORA<sup>8</sup>, A. DI CECCO<sup>2,4</sup>, S. DEGL'INNOCENTI<sup>9,10</sup>, I. FERRARO<sup>2</sup>, M. NONINO<sup>11</sup>,  
A. PIETRINFERNI<sup>12</sup>, L. PULONE<sup>2</sup>, P.G. PRADA MORONI<sup>9,10</sup>, M. ROMANIELLO<sup>6</sup>, N. SANNA<sup>2,4</sup>, AND A.R. WALKER<sup>13</sup>

(Dated: drafted 2018 November 9 / Received / Accepted)  
*Draft version 2018 November 9*

### ABSTRACT

We present accurate new ultraviolet and optical *BVI* photometry for the Galactic globular cluster NGC 2808, based on both ground-based and archival HST imagery. From this we have selected a sample of  $\sim 2,000$  HB stars; given the extensive wavelength range considered and the combination of both high-angular-resolution and wide-field photometric coverage, our sample should be minimally biased. We divide the HB stars into three radial bins and find that the relative fractions of cool, hot and extreme HB stars do not change radically when moving from the center to the outskirts of the cluster: the difference is typically smaller than  $\sim 2\sigma$ . These results argue against the presence of *strong* radial differentiation among any stellar subpopulations having distinctly different helium abundances. The ratio between HB and RG stars brighter than the ZAHB steadily increases when moving from the innermost to the outermost cluster regions. The difference is larger than  $\sim 4\sigma$  and indicates a deficiency of bright RGs in the outskirts of the cluster.

*Subject headings:* globular clusters: general — globular clusters: individual (NGC2808) — stars: horizontal-branch

### 1. INTRODUCTION

The Galactic globular cluster (GGC) NGC 2808 is a very interesting stellar system. Space- and ground-based optical photometry show that both the red giant branch (RGB) and the main sequence (MS) show spreads in color larger than can be explained by intrinsic photometric errors (Bedin et al. 2000). However, recent accurate high-resolution spectroscopic measurements of  $\sim 120$  RGs (Carretta 2006) indicate that no spread in metal abundance is present ( $[\text{Fe}/\text{H}] = -1.10 \pm 0.065$ ). The observational scenario was enriched by the detection of a fringe of stars blueward of the canonical MS by D'Antona et al. (2005). This evidence was solidified by the identification of a triple MS by Piotto et al. (2007) using accurate photometry of an off-center field collected with the Advanced Camera for Surveys (ACS) on board the Hubble Space Telescope (HST). The authors proposed that this cluster had experienced different episodes of star formation with significant helium enrichment ( $0.30 \leq Y \leq 0.40$ ).

NGC 2808 also shows an extended blue HB with multi-

ple distinct components, and a helium enrichment sufficient to explain the presence of multiple MSs had already been proposed to explain this morphology (D'Antona et al. 2002,2005; Lee et al. 2005). More recently, D'Ercole et al. (2008) have performed detailed simulations of the formation and the dynamical evolution of GCs hosting multiple stellar populations. They found that a substantial fraction of first generation stars are lost during the early cluster evolution. Moreover, the resulting radial profile of the ratio between second and first generation MS stars is characterized by a flat trend in the inner regions with a decrease (i.e., the first generation relatively more important compared to the second) in the outer cluster regions (see especially their Fig. 18).

From analysis of optical and UV Wide Field Planetary Camera 2 (WFPC2) images, Castellani et al. (2006) found that the ratio between HB and RG stars brighter than the HB luminosity level (the classical *R* parameter) in NGC 2808 increases when moving from the core to the outermost regions. A deficiency of bright RGs in this cluster was suggested by Sandquist & Martel (2007) on the basis of HST images. Peculiar radial distributions of HB stars in  $\omega$  Centauri have been suggested by Castellani et al. (2007). More recently, Zoccali et al. (2009) argued that the fainter (peculiar) of the two subgiant branches detected in NGC 1851 (Milone et al. 2008; Casisi et al. 2008) disappears at radial distances larger than 2.4 arcmin.

In this investigation we focus our attention on the luminosity function of HB stars in NGC 2808.

### 2. OBSERVATIONS AND DATA REDUCTION

In order to address these issues we took advantage of several UV and optical datasets collected with both HST and ground-based telescopes. These include UV data from the Space Telescope Imaging Spectrograph (STIS, 8511, PI: P. Goudfrooij) in far-UV (*FUV*, *F25QTZ*,  $\lambda_c =$

arXiv:0903.4531v1 [astro-ph.GA] 26 Mar 2009

<sup>1</sup> Based on observations collected with the ACS, WFPC2 and STIS on board of the Hubble Space Telescope.

<sup>2</sup> INAF-OAR, via Frascati 33, Monte Porzio Catone, Rome, Italy; giacinto@mporzio.astro.it

<sup>3</sup> IAC, Calle Via Lactea, E38200 La Laguna, Tenerife, Spain

<sup>4</sup> UniToV, Dipartimento di Fisica, via della Ricerca Scientifica 1, 00133 Rome, Italy

<sup>5</sup> DAO-HIA, NRC, 5071 West Saanich Road, Victoria, BC V9E 2E7, Canada

<sup>6</sup> ESO, Karl-Schwarzschild-Str. 2, 85748 Garching bei Munchen, Germany

<sup>7</sup> PUC, Departamento de Astronomia y Astrofisica, Casilla 306, Santiago 22, Chile

<sup>8</sup> INAF-OACN, via Moiariello 16, 80131 Napoli, Italy

<sup>9</sup> Univ. Pisa, Dipartimento di Fisica, Largo B. Pontecorvo 2, 56127 Pisa, Italy

<sup>10</sup> INFN-Pisa, via E. Fermi 2, 56127 Pisa, Italy

<sup>11</sup> INAF-OAT, via G.B. Tiepolo 11, 40131 Trieste, Italy

<sup>12</sup> INAF-OACTe, via M. Maggini, 64100 Teramo, Italy

<sup>13</sup> CTIO-NOAO, Casilla 603, La Serena, Chile

1590, FWHM=220 Å) and near-UV (NUV,  $F25CN270$ ,  $\lambda_c = 2700$ , FWHM=350 Å) bandpasses (Brown et al. 2001; Dieball et al. 2005,2009). Individual images cover a field of view (FoV) of  $25'' \times 25''$ , and the pixel scale is  $0''.0248/\text{px}$ . The entire data set consists of 18 FUV and 18 NUV images with exposure times ranging from 480 to 538s located across the cluster center (pointing  $\alpha$ , see Fig 1). We also used data from the ACS High Resolution Channel (ACS HRC, 10335, PI: H. Ford) in  $F435W$  ( $24 \times 135$  s) and  $F555W$  ( $4 \times 50$  s). Individual images cover a FoV of  $29'' \times 26''$  and the pixel size is  $0''.028 \times 0''.025$ . These images, too, are located across the cluster center (pointing  $\beta$ , Sandquist & Martel 2007). We also used data collected with ACS Wide Field Camera (ACS WFC, 10775, PI: A. Sarajedini) in  $F606W$  ( $5 \times 360$  s and  $1 \times 23$  s) and  $F814W$  ( $5 \times 370$  s +  $1 \times 23$  s). Individual images span  $202'' \times 202''$  at  $0''.05/\text{px}$ ; these are slightly dithered and are also located across the cluster center (pointing  $\epsilon$ ). These data were supplemented with optical/UV data images from the WFPC2: pointing  $\gamma$ , located near the cluster center—  $F218W$  ( $1 \times 1600$  s +  $1 \times 1700$  s),  $F439W$  ( $2 \times 230$  s +  $1 \times 50$  s),  $F555W$  ( $1 \times 7$  +  $1 \times 50$  s) from proposal 6095 (PI: S.G. Djorgovski; also Bedin et al. 2000; Castellani et al. 2006; Sandquist & Hess 2008); pointing  $\delta_i$ , also close to the cluster center and partially overlapping  $\gamma$ —  $F336W$  ( $2 \times 3600$  s),  $F555W$  ( $3 \times 100$  s +  $2 \times 7$  s),  $F814W$  ( $3 \times 120$  s +  $2 \times 3$  s) from proposal 6804 (PI: F. Fusi Pecci); pointing  $\delta_o$ , a couple of arcminutes southwest of the cluster center—  $F336W$  ( $4 \times 1600$  s),  $F555W$  ( $4 \times 900$  s +  $3 \times 100$  s +  $2 \times 7$  s),  $F814W$  ( $4 \times 700$  s +  $3 \times 120$  s +  $2 \times 3$  s), also from proposal 6804.

For wider coverage of the cluster regions, we collected multiband ( $UBVI$ ) ground-based archival data covering  $\approx 20' \times 15'$  around the center of the cluster (pointing  $\zeta$ , see Fig. 1). The dark area around the cluster centre marks the high density cluster regions. A total of 573 CCD images collected between 1987 January and 2002 February were reduced, but not all of these could be calibrated because of an insufficiency of standard-star observations. Moreover, since some of these data were acquired with mosaic cameras, and since even for single-chip cameras not all telescope pointings were the same, no individual star could be measured in all images. To summarize, calibrated photometry for any given star is available from at most 18 CCD images in  $U$ , 26 in  $B$ , 66 in  $V$ , and 59 in  $I$ .

Photometric reduction of the STIS images was done with ROMAFOT, while photometry of pointing  $\gamma$  was obtained with both ROMAFOT and DAOPHOT/ALLFRAME. The photometry for all the other data was carried out with DAOPHOT/ALLFRAME. The final catalog includes  $\sim 379,000$  stars with at least one measurement in two or more different optical bands,  $\sim 100,000$  stars with at least one  $U$  or  $F336W$  measurement, and  $\sim 4,900$  stars with at least one shorter-wavelength UV measurement ( $FUV$ ,  $NUV$ ,  $F218W$ ).

The WFPC2 photometry was kept in the Vega system following the prescriptions suggested by Holtzman et al. (1995). The STIS photometry was referred to the Vega system following the prescriptions by Brown et al. (2001) and Dieball et al. (2005). For homogeneity the ACS  $F435W$ ,  $F555W$ ,  $F606W$  and  $F814W$  magnitudes were

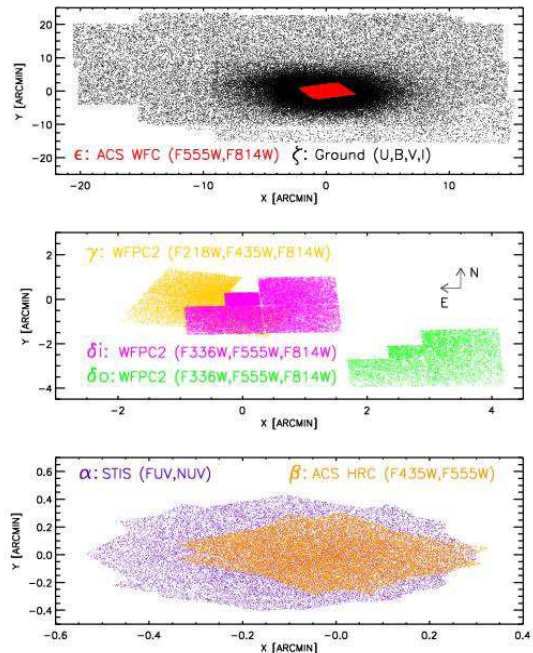


FIG. 1.— Top — multiband data collected with ACS@HST (WFC,  $F555W$ ,  $F814W$ ) and ground-based telescopes ( $U, B, V, I$ ). Middle — same as the top, but for data collected with WFPC2@HST ( $F218W$ ,  $F336W$ ,  $F555W$ ,  $F814W$ ). Bottom — same as the top, but for data collected with STIS@HST ( $FUV$ ,  $NUV$ ) and with ACS@HST (HRC,  $F435W$ ,  $F555W$ ). The arrows mark the Northern-Eastern directions.

transformed into WFPC2  $F435W$ ,  $F555W$  and  $F814W$  magnitudes on the basis of common stars. Finally, for the same reason, the ground-based  $UBVI$  magnitudes were transformed into the WFPC2  $F336W$ ,  $F435W$ ,  $F555W$  and  $F814W$  systems. The typical accuracy of the calibration is of the order of 0.02 mag for all the quoted bands. Here, however, we would like to stress that the results of the present paper depend upon *star counts* in different, easily recognized zones of the Color-Magnitude Diagrams (CMDs). Accuracy of the absolute calibrations is not a serious consideration for the present analysis.

### 3. RESULTS AND DISCUSSION

To identify HB stars near the center of the cluster we adopted the optical and UV results from HST. The reason is twofold. *i*) Detectors with a high angular resolution are mandatory for accurate photometry in crowded cluster regions. Note that the core radius and the half mass radius of NGC 2808 are  $r_c = 0.26$  and  $r_h = 0.76$  arcmin (Harris 1996<sup>14</sup>), respectively. Fortunately, these regions are covered by data sets collected with four different detectors (STIS, ACS HRC, ACS WFC, WFPC2). *ii*) The optical-UV colors are highly sensitive to effective temperature, providing the opportunity to properly select hot HB stars. For these reasons we gave the highest priority to CMDs based on optical-UV magnitudes. In particular, we adopted  $F555W, FUV-F555W$ ;  $F555W, NUV-F555W$ ;  $F555W, F218W-F555W$ ; and  $F555W, F336W-F555W$

<sup>14</sup> <http://physun.physics.mcmaster.ca/harris/mwgc.dat>

CMDs<sup>15</sup>. Data plotted in Fig. 2 show that the difference in color between Extreme HB (EHB) and RG stars ranges from  $\sim 6$  (panel d) to  $\sim 14$  mag (panel a). Moreover, they also show that in the UV bands (panels a,b,c) we detected not only HB stars but also Blue Stragglers ( $17.5 \lesssim F555W \lesssim 19$ ,  $1 \lesssim F218W - F555W \lesssim 2$ ), turnoff stars (TO, see the arrow in Fig. 2), main-sequence stars (MS), and a handful of bright RG stars. To our knowledge these are the deepest optical-UV CMDs ever collected for a GC.

Following Castellani et al. (2006) we define red HB (RHB) stars as those with colors redder than the RR Lyrae instability strip and with  $15.70 \leq F555W \leq 16.61$  mag. The HB stars bluer than the instability strip range from 15.8 to 21.6 in  $V$  or  $F555W$  magnitude, and we confirm the finding of Bedin et al. (2000) that they can—with minimal ambiguity—be divided into three subsets by cuts near  $V \sim F555W \sim 18.26$  and 19.95. From brightest to faintest, we refer to these three subgroups as EBT1, EBT2, and EBT3. The stars belonging to EBT3 have been called by different names in the literature (Moehler et al. 2004; Dalessandro et al. 2008), but we adopt our present nomenclature because we do not want to address their physical nature in this investigation. Note that in panel d) the RR Lyrae gap is not clearly identified, so to distinguish RHB from EBT1 stars we adopted either the  $F435W - F555W$  or the  $F555W - F814W$  color.

To avoid possible biases in the selection criteria and to improve the coverage of the inner cluster regions we also considered purely optical CMDs based on HST data: in particular,  $F555W, F439W - F555W$  and  $F555W, F555W - F814W$ . Finally, to cover the area between the inner regions covered by HST data and the tidal radius ( $r_t = 15.5$  arcmin) we adopted the  $F555W, F555W - F814W$  and the  $F555W, F336W - F814W$  CMDs inferred from ground-based photometry (see panel c,d of Fig. 3). Data plotted in Fig. 3 show that the current optical photometry provides very good sampling from the tip of the RGB down to a couple of magnitudes fainter than the TO. Despite NGC 2808’s low Galactic latitude ( $l^{\text{II}} = 282^\circ$ ,  $b^{\text{II}} = -11^\circ$ , the EBT1, EBT2, and EBT3 samples should be minimally contaminated by field stars, since stars this hot and faint are rare); conversely, RHB stars have  $F555W - F814W$  and  $F336W - F814W$  colors similar to common field stars.

Data plotted in the pure optical CMDs—panel d) of Fig. 2 and panel a), b), c) of Fig. 3—show that only a small fraction of the stars we have identified as probable HB stars could be confused with either MS or RG stars. Another small fraction of the HB sample lies among the stars located between the HB and the MS-RG fiducial cluster sequence. These stars appear to be normal HB stars in optical-UV CMDs. They were labeled “HB peculiar” by Castellani et al. (2006) and are probably either chance blends or physical binaries (Sandquist & Hess 2008).

Overall, we ended up with a sample of  $\approx 2,000$  HB stars distributed over the entire body of the cluster. Note that the current sample is almost a factor of two larger than the sample collected by Castellani et al. (2006). To

investigate their radial distribution, we split the total sample into three subgroups, namely  $r \leq r_a = 0.59$ ,  $r_a < r \leq r_b = 1.37$  and  $r_b < r \leq r_t = 15.5$  arcmin. The reason for specifically select these radial limits is twofold: *i*) each radial bin includes approximately 1/3 of the entire sample; *ii*) the two inner radial bins are based on HST data alone.

The lefthand panels of Fig. 4 show the Luminosity Function (LF) of the HB stars in the three different radial bins. The observed distributions (dotted lines) were smoothed using a conservative Gaussian kernel with standard deviation equal to three times the formal photometric uncertainties of individual stars to produce the solid curves. The vertical dashed lines show the range in apparent magnitude for the different HB groups, namely the RHB, which dominates the narrow peak, and the three EHB subgroups. These data (see also Table 1) indicate that, within the errors, the four HB subgroups follow the same radial distribution when moving from the center to the outskirts of the cluster. Moreover, more than 50% of all HB stars belong to the blue tail everywhere in the cluster. Data plotted in the right panels of Fig. 4 show that  $F814W$ -band LFs show very similar trends for the four subgroups when moving from the center to the outermost cluster regions (see also Table 1).

The apparent increase in the relative fraction of RHB stars in the external radial bin is caused by field star contamination. To evaluate their contribution on a quantitative basis we selected a region located well beyond the tidal radius ( $r \approx 19.4$  arcmin), and using both the  $F555W, F555W - F814W$  and the  $F555W, F336W - F814W$  CMD we found that we expect  $\approx 52 \pm 7$  field stars in the CMD box we adopted to define the RHB. The uncertainty claimed here accounts only for the Poisson uncertainty, and not for any (unexpected) nonuniform distribution of field stars. Once we subtract these stars from the external RHB group the relative fraction is still larger than for the inner two zones, but the difference is now smaller than  $1.5 \sigma$ . The external EBT1 group may show a slight deficiency compared to the inner zones, but again the anomaly is only of order  $\sim 1.5\sigma$  ( $F555W$ ) to  $\sim 2\sigma$  ( $F814W$ ). The other subgroups present similar differences, with no obvious overall pattern.

The above experiments indicate that the quantitative HB morphology in NGC 2808 does not show any pronounced radial trend. Moreover, the *qualitative* HB morphology (i.e., clumps and gaps) also does not change when moving from the very center to the outermost cluster regions, in agreement with the findings of Walker (1999) and Bedin et al. (2000). This evidence indicates either that the physical mechanism(s) driving the origin of the extended blue tail is at work across the entire body of the cluster, or that any putative subpopulations within the cluster are well mixed, in contrast with the predictions of D’Ercole et al. (2008; see also Yoon et al. 2008). Moreover, the apparent constancy of the HB with radius suggests that responsibility for the radial change in the ratio of HB to RG stars (Castellani et al. 2006) may lie with the RGs. To validate this working hypothesis we performed detailed counts of bright RGs using HST CMDs for the inner regions (see panel d) of Fig 2 and panels a,b of Fig. 3), and ground-based CMDs for the area located between the inner regions and the tidal radius (panels c,d of Fig. 3). Following Castellani et al. (2006)

<sup>15</sup> Note that we used weighted averages for the magnitudes of stars present in multiple data sets.

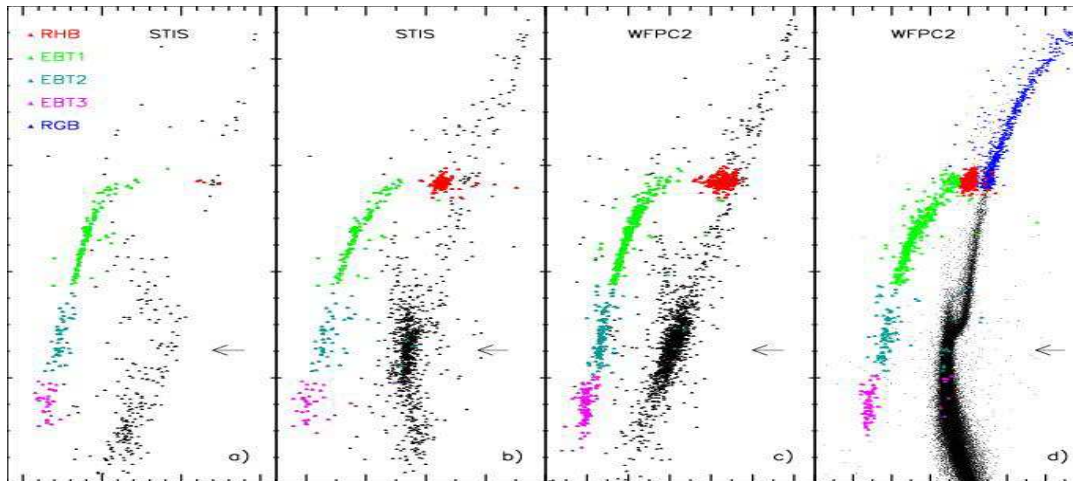


FIG. 2.— Optical-UV CMDs of NGC 2808 based on data collected with HST:  $F555W$ ,  $FUV-F555W$  (a),  $F555W$ ,  $NUV-F555W$  (b),  $F555W$ ,  $F218W-F555W$  (c),  $F555W$ ,  $F336W-F555W$  (d). Red, green, cyan and purple dots show different HB subgroups, while blue dots display RGB stars. The horizontal arrows mark the luminosity of Tur-Off stars ( $F555W = 19.82 \pm 0.02$  mag).

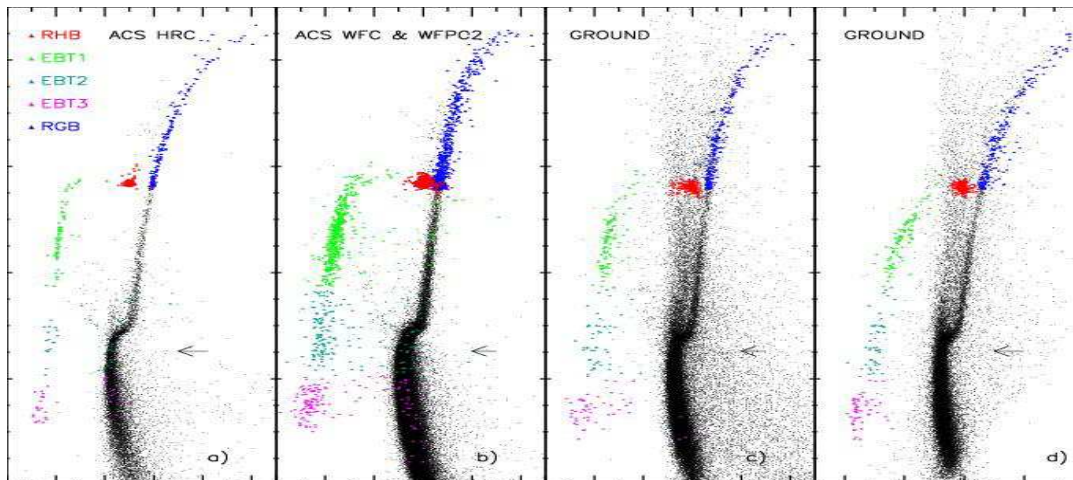


FIG. 3.— Same as Fig. 2, but for data sets collected with HST and with ground-based telescopes:  $F555W$ ,  $F439W-F555W$  (a),  $F555W$ ,  $F555W-F814W$  (b),  $F555W$ ,  $F555W-F814W$  (ground, c),  $F555W$ ,  $F336W-F814W$  (ground, d). Red, green, cyan and purple dots mark different subgroups of HB stars. The color coding of HB and RGB stars is the same as in Fig. 2. Data covering the external cluster regions show the contamination of field stars for  $14.5 \lesssim F555W \lesssim 19$ ,  $0.4 \lesssim F555W-F814W \lesssim 1.0$  (c) and for  $14.5 \lesssim F555W \lesssim 19$ ,  $1 \lesssim F336W-F814W \lesssim 2.0$ . (d). we adopted  $F555W_{ZAHB} = 16.43$  (VEGAMAG) and the same radial bins adopted for HB star counts. The field star contamination in the external radial bin was estimated using the same approach devised for RHB stars and we expect to find  $\approx 49 \pm 7$  field stars in the CMD box adopted to define bright RGs. Data listed in Table 1 show that the number of RGs steadily decreases from 444 for  $r \leq r_\alpha$  to 232 for  $r_\beta \leq r \leq r_t$ . The total number of RGs we detected is 40% larger than the number found by Castellani et al. (2006). Interestingly enough, the  $R$  parameter, i.e. the ratio between HB and RG stars brighter than the ZAHB, increases from  $1.32 \pm 0.08$  to  $2.76 \pm 0.21$  (see Table 1). The difference is larger than  $5\sigma$  and confirms the trend found by Castellani et al. (2006). To further constrain these findings we performed the same RG counts, but using the  $F814W$ -band. Data listed in

Table 1 show the same trend for RGs and the difference in the  $R$  parameter between the innermost and the outermost radial bin is larger than  $4\sigma$ . The current evidence indicates a deficiency of bright RGs in the outermost cluster regions.

#### 4. ACKNOWLEDGMENTS

It is a real pleasure to thank an anonymous referee for his/her positive comments and insights. We also thank S. Cassisi for many useful discussions and a detailed reading of an early draft of this paper. This project was partially supported by MIUR PRIN 2007 (PI: G. Piotto), INAF PRIN 2006 (PI: M. Bellazzini), Fondecyt Regular #1085278, the Fondap Center for Astrophysics #15010003, and by the BASAL CATA.

#### REFERENCES

TABLE 1  
THE HB AND RGB STAR COUNTS IN DIFFERENT RADIAL BINS. NUMBERS IN BRACKETS ARE THE RELATIVE FRACTIONS OF THE HB SUBGROUPS.

Radius	N(RHB)	N(EBT1)	N(EBT2)	N(EBT3)	$N(HB)$	$N(RGB)^a$	$R^b$
Star counts based on the $F555W$ -band LF <sup>c</sup>							
$r \leq r_a$	217 (37 ± 3%)	217 (37 ± 3%)	81 (14 ± 2%)	69 (12 ± 1%)	584	444	$1.32 \pm 0.08$
$r_a < r \leq r_b$	238 (35 ± 3%)	244 (36 ± 3%)	112 (16 ± 2%)	88 (13 ± 1%)	682	340	$2.01 \pm 0.13$
$r_b < r \leq r_t$	360 (52 ± 3%)	164 (24 ± 2%)	84 (12 ± 1%)	85 (12 ± 1%)	693	281	$2.47 \pm 0.17$
Total	815 (42 ± 2%)	625 (32 ± 2%)	277 (14 ± 1%)	242 (12 ± 1%)	1959	1065	$1.84 \pm 0.07$
$r_b < r \leq r_t^c$	308 (48 ± 4%)	164 (26 ± 2%)	84 (13 ± 1%)	85 (13 ± 1%)	641	232	$2.76 \pm 0.21$
Total <sup>c</sup>	763 (40 ± 3%)	625 (33 ± 2%)	277 (14 ± 1%)	242 (13 ± 1%)	1907	1016	$1.88 \pm 0.07$
Star counts based on $F814W$ -band LF <sup>d</sup>							
$r \leq r_a$	273 (41 ± 3%)	273 (41 ± 3%)	86 (12 ± 2%)	40 (6 ± 1%)	672	439	$1.53 \pm 0.09$
$r_a < r \leq r_b$	262 (37 ± 3%)	269 (37 ± 3%)	124 (17 ± 2%)	66 (9 ± 1%)	721	344	$2.10 \pm 0.14$
$r_b < r \leq r_t$	368 (52 ± 3%)	180 (25 ± 2%)	85 (12 ± 1%)	82 (11 ± 1%)	715	298	$2.40 \pm 0.17$
Total	903 (43 ± 2%)	722 (34 ± 2%)	295 (14 ± 1%)	188 (9 ± 1%)	2108	1081	$1.95 \pm 0.07$
$r_b < r \leq r_t^c$	316 (48 ± 4%)	180 (27 ± 2%)	85 (13 ± 1%)	82 (12 ± 1%)	663	249	$2.66 \pm 0.20$
Total <sup>c</sup>	851 (42 ± 3%)	722 (35 ± 2%)	295 (14 ± 1%)	188 (9 ± 1%)	2056	1032	$1.99 \pm 0.08$

<sup>a</sup> Star counts of RGs brighter than the ZAHB, i.e. RGs brighter than either  $F555W=16.43$  or  $F814W=15.33$  mag.

<sup>b</sup> R parameter, i.e. the ratio between HB and RGs brighter than the ZAHB. The error only accounts for the Poisson uncertainty.

<sup>c</sup> Star counts of the external radial bin cleaned for field star contamination in the RHB group.

<sup>d</sup> The limits adopted in the  $F814W$ -band to identify the HB subgroups are: RHB – redder than RR Lyrae and  $14.75 \leq F814W \leq 15.77$ , EBT1 – bluer than RR Lyrae and  $15.77 < F814W \leq 18.21$ , EBT2 –  $18.21 < F814W \leq 19.89$ , EBT3 –  $19.89 < F814W \leq 21.50$ .

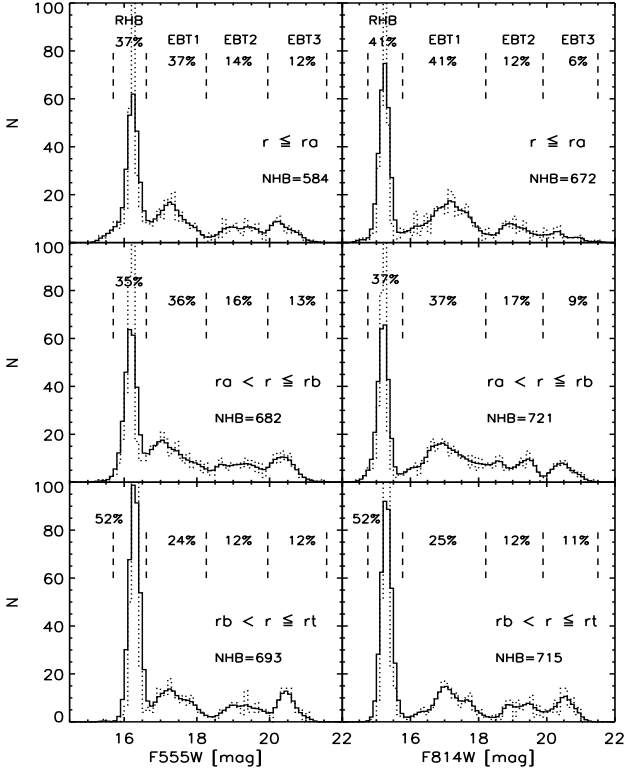


FIG. 4.— Luminosity function of HB stars in the  $F555W$  (left) and in the  $F814W$ -band (right). From top to bottom the three panels display the luminosity function in different radial bins. The dotted lines display the observed distributions, while the solid lines the smoothed luminosity function obtained using a Gaussian kernel. The vertical dashed lines show the magnitude ranges adopted to select the HB subgroups. The number of HB stars per bin and the relative fractions of HB subgroups are also labeled.

Carretta, E. 2006, AJ, 131, 1766  
 Cassisi, S., et al. 2008, ApJ, 672, L115  
 Castellani, V., et al. 2006, A&A, 446, 569  
 Castellani, V., et al. 2007, ApJ, 663, 1021  
 Dalessandro, E., et al. 2008, ApJ, 681, 311  
 D'Antona, F., et al. 2002, A&A, 395, 69  
 D'Antona, F., et al. 2005, AJ, 631, 868  
 D'Ercole, A., et al. 2008, MNRAS, 391, 825  
 Dieball, A., et al. 2005, ApJ, 625, 156  
 Dieball, A., et al. 2009, MNRAS, 394, L56  
 Harris, W. E. 1996, AJ, 112, 1487  
 Holtzman, J. A., et al. 1995, PASP, 107, 1065  
 Lee, Y.-W., et al. 2005, AJ, 621, L57  
 Milone, A. P., et al. 2008, ApJ, 673, 241  
 Moehler, S., et al. 2004, A&A, 420, 515  
 Piotto, G., et al. 2007, ApJ, 661, L53  
 Sandquist, E. L., & Martel, A. R. 2007, ApJ, 654, L65  
 Sandquist, E. L., & Hess, J. M. 2008, AJ, 136, 2259  
 Walker, A. R. 1999, AJ, 118, 432  
 Yoon, S.-J. et al. 2008, ApJ, 677, 1080  
 Zoccali, M., et al. 2009, ApJ, accepted, arXiv0901.4476